X-RAY SPECTROMETRY
*X-Ray Spectrom.* 2002; **31**: 209–218
Published online in Wiley InterScience (www.interscience.wiley.com). DOI: 10.1002/xrs.528

XRS

# Accuracy of the fundamental parameter method for x-ray fluorescence analysis of rocks†

**V. Ya. Borkhodoev***

North-East Interdisciplinary Science Research Institute of the Russia Academy of Sciences Far East Branch, 16, Portovaya SVKNII, 685000 Magadan, Russia

Received 20 February 2001; Accepted 29 June 2001

**The accuracy of quantitative X-ray fluorescence (XRF) analysis of rocks by means of the fundamental parameter (FP) method is predetermined by the completeness of the characteristic X-radiation model, the degree of uncertainty in the FPs and the correctness of the calculation algorithms. This paper contains the results of a study of these factors for the XRF analysis of rocks that differ greatly in their elemental compositions. In order to improve the model of characteristic X-radiation, the significance of photoelectrons is thoroughly examined in this paper, and the effects of divergence of the primary radiation beam is assessed. The FP uncertainties are studied in this paper, and equations are derived to calculate the fluorescence yield, probabilities of serial line radiation and absorption jumps. Equations are proposed to calculate the mean electron energy and spectral intensity of X-ray tube radiation. A numerical integration algorithm is optimized by wavelengths, with allowance for the X-ray tube bremsstrahlung radiation. A software program is developed to calculate the characteristic radiation intensity and element compositions. Metrologic characteristics of the FP method based XRF analysis allow for its use in rock studies.** 

## INTRODUCTION

The use of X-ray fluorescence(XRF) analysis in geology and geochemistry is limited owing to the lack of this analytical procedures flexibility under significant matrix variations. Such a restriction can be removed by using the fundamental parameter (FP) method, which is based on sound physical principles and is all-round with regard to materials examined and elements determined.

Among the XRF analysis methods, the FP method is unique. It is based on an equation that describes the characteristic X-radiation intensity of the sample atoms. The successful use of the XRF method is directly related to the completeness of the characteristic X-radiation model, the degree of uncertainty of the FP and the correctness of the calculation algorithm. Therefore, an accurate quantitative analysis by virtue of the FP method is possible only if all the above-mentioned characteristics are improved. The FP method algorithm and the results of its use in practice have already been described.[1] This paper represents further studies in this area and the results obtained.

## THE CHARACTERISTIC X-RADIATION MODEL FOR XRF ROCK ANALYSIS

### Introduction

The analytical line intensity is represented as follows:

$$I_i = I_i^{\mathrm{P}} + I_i^{\mathrm{S}} + I_i^{\mathrm{T}} + I_i^{\mathrm{Sc}} + I_i^{\mathrm{Ph}} + I_i^{\mathrm{A}} \tag{1}$$

where $I_i^{\mathrm{P}}$, $I_i^{\mathrm{S}}$ and $I_i^{\mathrm{T}}$ are the intensities of the primary, secondary and tertiary fluorescence respectively; $I_i^{\mathrm{Sc}}$, $I_i^{\mathrm{Ph}}$ and $I_i^{\mathrm{A}}$ are the intensities of the analytical line radiation excited by scattered radiation, photoelectrons and Auger electrons respectively.

In this paper, the equations from Sherman,[2] Pavlinsky and Losev,[3] Shiraiwa and Fujino[4] and Afonin and Gunicheva[5] are used to express $I_i^{\mathrm{P}}$ and $I_i^{\mathrm{S}}$. With allowance for the secondary XRF, the intensity of the analytical line is summed up as the follows:

$$I_i = I_i^{\mathrm{P}} + I_i^{\mathrm{S}} \tag{2}$$

When the XRF is excited both by bremsstrahlung and the characteristic radiation of the X-ray tube, we have the following:

$$I_i^{\mathrm{P}} = w_{qi} c_i F_i \tag{3}$$

where

$$F_i = \int_{\lambda_0}^{\lambda_{qi}} \frac{N(\lambda)\mu_{\lambda i}\,\mathrm{d}\lambda}{\mu_\lambda/\sin\varphi + \mu_i/\sin\psi} \tag{4}$$

$$N(\lambda) = N_\lambda + \sum_l \delta(\lambda - \lambda_l) N_l \tag{5}$$

where $c_i$ is the weight fraction of an element $i$, $w_{qi} = p_{qi}^k \omega_{qi} r_{qi}$; $\mu_{\lambda i}$ and $\mu_\lambda$ are the mass attenuation coefficients (MACs) for the primary radiation, with wavelength $\lambda$, of element $i$ and the sample respectively; $\mu_i$ is the MAC for the sample analytical line radiation; $\omega_{qi}$ is the fluorescence yield; $p_{qi}^k$ is the probability of radiation of analytical line $k$ of element $i$; $r_{qi}$ is the absorption jump factor; $\varphi$ is the angle between the central beam of X-radiation from the source and the surface of the

*Correspondence to: V. Ya. Borkhodoev, North-East Interdisciplinary Science Research Institute of the Russia Academy of Sciences For East Branch, 16, Portovaya SVKNII, 685000 Magadan, Russia.
†Special Issue on X-Ray Methods in Countries of the Former Soviet Union.

sample; $\psi$ is the take-off angle of secondary radiation; $N_\lambda$ and $N_l$ are the intensities of the continuous and characteristic radiation of the X-ray tube; $\lambda_0$ is the short-wavelength limit of the continuous spectrum; and $\lambda_{qi}$ is the absorption edge of element $i$.

The intensity of the analytical line of element $i$ excited by primary fluorescence of element $j$ is obtained by the following formula:

$$I_{ij}^{S} = 0.5 c_i w_{qi} c_j w_{qj} \mu_{ji} \Phi_j \tag{6}$$

where

$$\Phi_j = \int_{\lambda_0}^{\lambda_{qj}} \frac{N(\lambda)\mu_{\lambda j} L_\lambda \, d\lambda}{\mu_\lambda / \sin\varphi + \mu_i / \sin\psi} \tag{7}$$

$$L_\lambda = \frac{\sin\varphi}{\mu_\lambda} \ln\left(1 + \frac{\mu_\lambda}{\mu_j \sin\varphi}\right) + \frac{\sin\psi}{\mu_i} \ln\left(1 + \frac{\mu_i}{\mu_j \sin\psi}\right) \tag{8}$$

where $w_{qj} = r_{qj}\omega_{qj}p_{qj}^k$; $c_j$ is the $j$-element weight fraction; $\mu_{\lambda j}$ is the MAC of element $j$ for the primary radiation; $\mu_{ji}$ is the MAC of element $j$ for the characteristic radiation of element $i$; and $\mu_j$ is the MAC of element $j$ radiation by the sample.

If $i$-element fluorescence can be excited by $n$ elements of a sample, then, it follows that

$$I_i^{S} = \sum_{j=1}^{n} I_{ij}^{S} \tag{9}$$

When deriving Eqn (9), the assumption is made that the entire radiation of element $j$ occurs as one line.

Other components are insignificant for rock XRF analysis.[5,6] But, as we believe, the role of photoelectrons in analytical radiation excitation is worthy of being made more precise.

## Effect of photoelectrons

The energy of photoelectrons $E_j^{Ph}$ equals the energy of photons of primary radiation $E_\lambda$ minus the ionization energy of the $q$-shell of element $j$: $E_{qj}$, i.e. $E_j^{Ph} = E_\lambda - E_{qj}$. The spectrum of the photoelectrons is the same as that of the primary radiation, but shifted to the long-wave region for the $E_{qj}$ value. The maximum energy of the photoelectrons will be $E_j^{Ph} = E_0 - E_{qj}$; thus, it depends on atomic number $Z$ and on what atom shell is ionized by the primary radiation photons.

Equation (10) is obtained to express the intensity of the analytical line radiation excited by photoelectrons, which form under the interaction between primary bremsstrahlung radiation and the $q$-shell of element $j$ of an infinitely thick sample:

$$I_i^{Ph} = c_i \omega_{qi} p_{qi}^k \sum_j c_j \sum_q r_{qj} D_j \tag{10}$$

where

$$D_j = \int_{\lambda_0}^{\lambda^*_{qij}} \frac{\tau_{\lambda j} N_\lambda P_{qi}(E_{j\lambda}^{Ph}) \, d\lambda}{\mu_\lambda / \sin\varphi + \mu_i / \sin\psi} + \sum_l \frac{N_l \tau_{lj} P_{qi}(E_{jl}^{Ph})}{\mu_l / \sin\varphi + \mu_i / \sin\psi} \tag{11}$$

where $\tau_{\lambda j}$ and $\tau_{lj}$ are the photoelectric cross-sections for $\lambda$ and $l$ wavelength radiation; $P_{qi}(E_{jl}^{Ph})$ is the number of $q$-shell ionizations; $\lambda^*_{qij} = \lambda_{qj}\lambda_{qi}/(\lambda_{qj} + \lambda_{qi})$.

The formula obtained differs from the others[7,8] in its form and integration limits.

The contribution of photoelectrons to the analytical lines excitation of some rock major and trace elements is assessed for monochromatic primary radiation conditions. In this group of elements, the K-line radiation is an order more intense than that of L lines; therefore, the calculation is made only for K photoelectrons, and the backscattering of electrons is ignored. Thus simplified, a formula is obtained assessing the photoelectron contribution to excitation of analytical line radiation:

$$\gamma_i^{Ph} = \frac{\sum_j c_j N_l \tau_{lj} P_{Ki}(E_{jl}^{Ph})}{N_l \tau_{li}} \tag{12}$$

Table 1 contains the calculated results for $\gamma_i^{Ph}$ values of four samples: standard reference materials (SRMs) SG-2,

**Table 1.** The $\gamma_i^{Ph}$ calculation results for Rh K$\alpha$ line exciting radiation conditions

| | | SG-2 | | SGD-1A | | | |
|---|---|---|---|---|---|---|---|
| $Z$ | $10^{-1}\lambda$ (nm) | undiluted | with $Li_2B_4O_7$ | undiluted | with $Li_2B_4O_7$ | with $Li_2B_4O_7$[a] | with $Li_2B_4O_7$[b] |
| 11 | 11.91 | 0.373 | 0.226 | 0.284 | 0.196 | 0.497 | 0.0036 |
| 12 | 9.89 | 0.199 | 0.121 | 0.151 | 0.105 | 0.292 | 0.0014 |
| 13 | 8.339 | 0.106 | 0.065 | 0.080 | 0.056 | 0.174 | 0.0005 |
| 14 | 7.125 | 0.063 | 0.038 | 0.047 | 0.033 | 0.107 | 0.000 05 |
| 15 | 6.157 | 0.036 | 0.022 | 0.027 | 0.019 | 0.065 | |
| 19 | 3.741 | 0.006 | 0.003 | 0.004 | 0.003 | 0.011 | |
| 20 | 3.358 | 0.004 | 0.002 | 0.003 | 0.002 | 0.008 | |
| 22 | 2.748 | 0.002 | 0.001 | 0.0012 | 0.0009 | 0.004 | |
| 25 | 2.101 | 0.0005 | 0.0003 | 0.0004 | 0.0003 | 0.001 | |
| 26 | 1.936 | 0.0004 | 0.0002 | 0.0003 | 0.0002 | 0.001 | |

[a] Primary radiation with wavelength $0.3719 \times 10^{-1}$ nm.

[b] Rh L$\alpha_1$ line primary radiation.

SGD-1A, and the same samples diluted with $Li_2B_4O_7$ with mass ratio 1 : 1. The calculation conditions are as follows: the primary radiation is the Rh K$\alpha$ line, $\varphi = 90^\circ$, $\psi = 40^\circ$. It appears that though the contributions of the diluted samples become less important, they remain significant for the K$\alpha$ line radiations of Na, Mg, Al and Si, reaching a maximum of 22.6%.

Indeed, the analytical line radiation is excited by both the characteristic and the bremsstrahlung X-ray tube radiation; so, it would be of research interest to us to analyse the changing effect value versus the wavelength of the primary radiation. Table 1 presents the $\gamma_i^{Ph}$ calculation results for the SGD-1A sample diluted with $Li_2B_4O_7$, under excitation conditions caused by a primary radiation of different wavelengths. The values of the additionally chosen wavelengths correspond to a maximum distribution of bremsstrahlung radiation ($0.3719 \times 10^{-1}$ nm) and the Rh L$\alpha_1$ line ($4.5974 \times 10^{-1}$ nm).

From the data in Table 1 it follows that: (1) as the energy of the primary radiation photons is decreased, the contribution of the photoelectrons to exciting the analytical line radiation of light elements is sharply decreased; (2) the photoelectron excitation effect obviously tends to be less significant as the atomic number of the elements determined becomes greater and samples are diluted; (3) diluted samples feature relatively insignificant changes of the above-mentioned effect, as their chemical composition changes from granite to gabbro rocks. These results serve as the basis for us to conclude the following: when the XRF of rock elements is excited by virtue of the mixed radiation of an X-ray tube, the photoelectron-excitation effect is insignificant, therefore, such an effect can be ignored, and the determination of element compositions will be just slightly erroneous.

## Divergence of primary beam

In this paper, the divergence effects of the primary radiation beam for the XRF intensity are assessed when an XRF analysis of rocks is performed. Under monochromatic primary radiation conditions, the relative intensity $R_i$ of the XRF of element $i$ is given, as a first approximation, by:

$$R_i = \frac{I_i}{I_i^{ref}} \approx \frac{c_i}{c_i^{ref}} \left( \frac{1 + K^{ref} x}{1 + Kx} \right) \frac{\mu_i^{ref}}{\mu_i} \qquad (13)$$

where

$$K^{ref} = \frac{\mu_i^{ref}}{\mu_1^{ref}} \frac{1}{\sin\psi} \quad K = \frac{\mu_i}{\mu_1} \frac{1}{\sin\psi}$$

and $x = \sin\varphi$. Superscripts 'ref' denote a reference sample.

The relative change of $R_i$ is calculated using Eqn (14):

$$\delta R_i = \frac{\Delta R_i}{R_i} = \frac{K^{ref} - K}{(1 + Kx)(1 + K^{ref} x)} \Delta x \qquad (14)$$

According to $\delta R$ calculation results for XRF excitation using monochromatic primary radiation of the Rh K$\alpha_1$, Rh L$\alpha_1$ and W L$\alpha_1$ lines, the $\delta R$ value depends on the wavelength of the primary radiation, i.e. the shorter the radiation wavelength the less significant the beam divergence is for a relative intensity. The divergence effect of the primary radiation beam grows correspondingly to a greater importance of a primary radiation weakening in a sample in comparison with a secondary radiation weakening.

On the basis of formulas by Pavlinsky and Kitov,[9] calculations were made of the $\varphi^{eff}$ effect angle and the $\eta$ correction coefficient of beam divergence for $Li_2B_4O_7$-diluted samples, with mass ratio 1 : 1. It is established that, when the $t$ parameter (which depends on the chemical composition of samples)[9] changes on the order of 3, the $\eta$ coefficient changes only by 2.7%. So, the primary radiation beam divergence being neglected, the calculation error of radiation intensities of rock element analytical lines is insignificant. The calculated effect angle $\varphi^{eff}$ is $75.3^\circ \pm 0.1^\circ$.

Under the experimental conditions of this study, the analytical line $R_i$ values are calculated for some elements of rock samples diluted with a filler (ABS-plastic 'STAN'), with mass ratio 1 : 1, with the primary radiation beam divergence $R_p$ allowed for (the angle between the central beam of the primary X-radiation from the source and the surface of the sample $\varphi$ is taken as $\varphi^{eff}$) and the beam divergence $R_d$ ignored ($\varphi = 90^\circ$). The reference sample is MK-1 SRM. The calculation results are given in Table 2. This shows that the relative errors $\delta$ found for analytical lines [the latter represent a significant wavelength interval from the Na K$\alpha_1$ line to the Sr K$\alpha_1$ line of different rock types ranging from granites (SG-1A, MK-3), to alkaline rocks (MSH-1-4) and ultrabasic rocks (MU-3)] are placed at the same level; therefore, when the XRF analysis of rocks is made, the divergence effects of the primary radiation beam can be neglected.

**Table 2.** Comparison of relative intensities of analytical line radiation calculated with and without account of the primary radiation beam divergence

| | Na K$\alpha_1$ | | | Si K$\alpha_1$ | | | Sr K$\alpha_1$ | | |
|---|---|---|---|---|---|---|---|---|---|
| SRM | $R_p$ | $R_d$ | $\delta$ (%) | $R_p$ | $R_d$ | $\delta$ (%) | $R_p$ | $R_d$ | $\delta$ (%) |
| MK-3 | 0.9618 | 0.9682 | 0.66 | 1.1530 | 1.1455 | 0.65 | 0.3377 | 0.3368 | 0.27 |
| MK-4 | 1.4139 | 1.4231 | 0.65 | 1.1350 | 1.1279 | 0.63 | 1.3954 | 1.3920 | 0.24 |
| SG-1A | 1.7937 | 1.8055 | 0.65 | 1.1983 | 1.1900 | 0.69 | 0.0503 | 0.0502 | 0.20 |
| ST-1A | 0.6597 | 0.6635 | 0.57 | 0.6951 | 0.6924 | 0.39 | 0.3899 | 0.3889 | 0.26 |
| MSH-1 | 2.7718 | 2.7882 | 0.59 | 0.8479 | 0.8431 | 0.57 | 0.2917 | 0.2910 | 0.24 |
| MSH-3 | 4.2814 | 4.3034 | 0.51 | 0.5701 | 0.5675 | 0.46 | 2.1246 | 2.1193 | 0.25 |
| MO-2 | 1.0563 | 1.0621 | 0.55 | 0.6909 | 0.6879 | 0.43 | 0.8269 | 0.8248 | 0.25 |
| MSH-4 | 1.2048 | 1.2116 | 0.56 | 0.7510 | 0.7475 | 0.47 | 1.4057 | 1.4022 | 0.25 |
| MU-3 | 0.5511 | 0.6638 | 0.49 | 0.4979 | 0.4963 | 0.32 | 0.3763 | 0.3754 | 0.24 |

## THE FPS STUDY

### MACs

The MAC values given in ten publications available[10–19] (hereinafter referred to in this text as the 'tables') are compared within the wavelength interval ranging from $1.936 \times 10^{-1}$ to $11.91 \times 10^{-1}$ nm. The author of this paper examined the radiation of Na, Mg, Al, Si, P, K, Ca, Ti, Mn, Fe, Zn and Sr K$\alpha$ lines attenuated with atoms of the above-mentioned elements and also of oxygen and flux and filler components (Li, B).

The spread in the MAC values given in the tables is taken as an actual uncertainty and estimated in terms of a relative standard deviation $s_r$. From 180 possible interactions between the radiation of the analytical K$\alpha$ lines of the petrogenic elements and the above-mentioned atoms, the spread in the MAC values has $s_r$ greater than 5% in 69 cases, greater than 10% in 27 cases, greater than 30% in nine cases, with a maximum of 61.7%.

In order to assess how a combined MAC uncertainty of some elements affects the calculation accuracy of XRF intensities, when many-component samples are analysed, the analytical line intensities $I_i$ of petrogenic elements are calculated with the use of data given in the different MAC tables in terms of an XRF monochromatic model:

$$I_i = c_i \frac{N_1 \mu_{1i}}{\mu_1 / \sin\varphi + \mu_i / \sin\psi}$$

where $\mu_{1i}$ is the MAC of element $i$ primary radiation.

Calculations are made for SG-2 granite and SGD-1A gabbro samples, under XRF conditions excited by a primary radiation of Rh K$\alpha_1$ and Rh L$\alpha_1$ lines, $\varphi = 90°$, $\psi = 40°$. Calculations are also made for samples diluted with $Li_2B_4O_7$, with mass ratio 1 : 1. The $R$ values are established as a relationship between the SG-2 intensities and the corresponding SGD-1A intensities. The spread in intensities, which is the result of using different MAC tables, is estimated by virtue of the $s_r$ value. The calculation results are given in Table 3.

It appears that the absolute intensity variations are significant and are of the same order, both for clean and diluted samples. The $s_r$ value tends to decrease as the analytical line wavelength becomes shorter. The $s_r$ values established for SRMs SG-2 and SGD-1A do not differ significantly, but the $s_r$ value obviously depends on the primary radiation wavelength. When the XRF is excited by the Rh L$\alpha_1$ line long-wave radiation, the $s_r$ value of the Mg K$\alpha_1$, Al K$\alpha_1$, and Si K$\alpha_1$ line intensities is two times and more less in comparison with the situation when excitation is a result of Rh K$\alpha_1$ line radiation. This testifies to the large contribution of the latter line MAC uncertainty to the spread of the calculation results.

The spread in the relative intensities is much less significant in comparison with that in the absolute intensities. The dilution technique causes a decrease in relative intensity variations, and this becomes especially obvious when long-wave analytical lines are analysed. The relative intensity calculation errors, which are due to the MAC uncertainty, can be compared with allowable errors in determinations of rock and mineral compositions.[20] The significant difference between spreads in absolute and relative intensities seems to be the result of inherent consistency of data from one table. It follows that, in order to minimize the calculation errors of intensities and contents, the MAC values for radiation of all wavelengths should be taken from the same table to solve a given problem.

To make calculations using Eqns (4) and (7) we must know the attenuation of radiation within the wavelength interval $[\lambda_0, \lambda_{qi}]$. While making determinations of petrogenic elements and microelements, the X-ray tube voltage was 50 kV. In this case, the MAC tables shall contain the radiation attenuation data ranging from $\lambda_0 = 0.247 \times 10^{-1}$ to $11.910 \times 10^{-1}$ nm (Na K$\alpha$ line). Such table data are available in some papers,[13,14,17,19] but there is no approximation formula in the table by Dewey *et al.*[13] that could be used to define a MAC value for any wavelength.

**Table 3.** The spread in intensities of petrogenic elements analytical lines $s_r$ calculated using different MAC tables, in %

| | | Non-diluted sample | | | Diluted sample | | |
|---|---|---|---|---|---|---|---|
| Primary radiation | Analytical line | SG-2 | SGD-1A | $R$ | SG-2 | SGD-1A | $R$ |
| Rh K$\alpha$ | Na K$\alpha$ | 3.0 | 4.3 | 2.1 | 3.2 | 3.6 | 1.2 |
| | Mg K$\alpha$ | 9.0 | 7.9 | 1.9 | 8.6 | 8.0 | 1.0 |
| | Al K$\alpha$ | 9.6 | 7.6 | 2.5 | 9.2 | 8.1 | 1.4 |
| | Si K$\alpha$ | 5.7 | 5.0 | 1.3 | 6.4 | 5.8 | 0.9 |
| | P K$\alpha$ | 2.5 | 2.9 | 1.0 | 3.4 | 3.9 | 0.8 |
| | K K$\alpha$ | 3.4 | 3.2 | 0.4 | 3.5 | 3.4 | 0.4 |
| | Ca K$\alpha$ | 2.1 | 1.9 | 0.7 | 2.0 | 1.9 | 0.6 |
| | Ti K$\alpha$ | 3.5 | 2.7 | 1.2 | 3.3 | 2.5 | 1.0 |
| | Mn K$\alpha$ | 2.5 | 1.7 | 0.9 | 2.5 | 1.8 | 0.8 |
| | Fe K$\alpha$ | 1.4 | 1.1 | 0.7 | 2.3 | 2.0 | 0.7 |
| Rh L$\alpha$ | Na K$\alpha$ | 3.2 | 4.3 | 1.9 | 3.1 | 3.6 | 1.1 |
| | Mg K$\alpha$ | 3.2 | 3.8 | 1.4 | 3.0 | 3.3 | 0.8 |
| | Al K$\alpha$ | 3.6 | 2.5 | 1.5 | 3.8 | 3.0 | 1.0 |
| | Si K$\alpha$ | 2.5 | 2.4 | 0.8 | 3.1 | 2.8 | 0.6 |
| | P K$\alpha$ | 2.3 | 2.8 | 0.7 | 3.4 | 3.9 | 0.6 |

The MAC uncertainty is expected to grow in the absorption jump area. The MAC values are calculated for Na, Mg, Al, Si, P, K, Ca, Ti, Mn, Fe, Zn and Sr elements on the basis of different table data, for their absorption jump areas and with a wavelength step of $0.05 \times 10^{-1}$ nm. The average MAC values and their $s_r$-described spreads before and after the absorption jumps are given in Table 4. Significant MAC deviations in the area of the Na, Al and Si K absorption edges are due to the wrong values of K absorption edges. If such rough errors are neglected, the spread in the MAC values within the absorption jump area lies within the interval $s_r = 2.2–11.4\%$.

Proceeding from the results obtained, we recommend that the tables of Storm and Israel,[14] Marenkov[17] and de Boer[19] be used for calculations of weakening of the bremsstrahlung component of the primary radiation when XRF analysis of rocks is undertaken, with the wavelength intervals covered by the tables.

## Other FPs

According to the $\omega_K$ data obtained from different sources, the uncertainty in the fluorescence yield becomes greater as the $Z$ numbers of the elements decreases. We believe it reasonable to characterize it not only as an average value, but also in terms of $s_r$, which is a measure of its uncertainty. We use data contained in 11 published papers[5,21–30] as a basis to calculate the mean values of $\omega_K$ and $s_r$ for elements having $Z$ from 3 to 92. Figure 1 shows the $\omega_K$ and $s_r$ values versus $Z$. Similar $\omega_L$ studies were made on the basis of seven papers, and the results obtained are shown in Fig. 2. Fluorescence yield data presented in four papers were analysed for the L3 subshell; the results are represented in Fig. 3.

The Gauss–Newton method is used to derive formulas that approximate the dependence of established mean $\omega_K$, $\overline{\omega}_L$, and $\omega_{L3}$ values on $Z$:

$$\omega_K = Z^4/(942\,532.6 + Z^4) \quad (15)$$

$$\overline{\omega}_L = 0.0809 - 0.005\,74Z + 0.000\,112Z^2 \quad (16)$$

$$\omega_{L3} = 0.0912 - 0.006\,18Z + 0.000\,114Z^2 \quad (17)$$

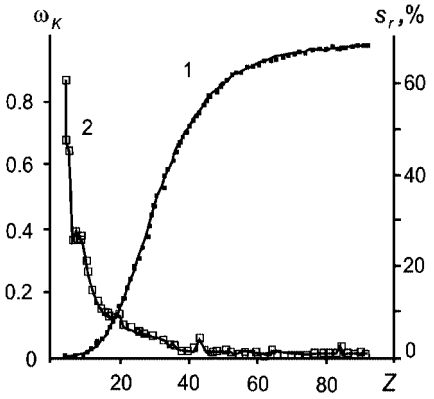


**Figure 1.** $\omega_K$ (1) and $s_r$ (2) values versus atomic number.

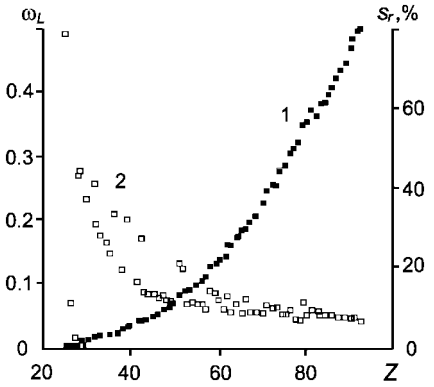


**Figure 2.** $\omega_L$ (1) and $s_r$ (2) values versus atomic number.

The calculation results obtained by virtue of these formulas agree with the table data and have the correlation coefficient more than 0.996.

The line radiation probabilities are calculated for the L series, and, on their basis, the following formula is obtained:

$$p_{Li} = a_0 + a_1Z + a_2Z^2 + a_3Z^3 \quad (18)$$

The calculated coefficients for the line radiation probabilities are given in Table 5. The radiation probabilities of the $L\alpha_1$,

**Table 4.** The mean values and spread in MAC elements before and after the K absorption jump

| | Mean values and spread in MAC | | | |
|---|---|---|---|---|
| | Before absorption jump | | After absorption jump | |
| Element | Mean ($cm^2/g^{-1}$) | $s_r$ (%) | Mean ($cm^2/g^{-1}$) | $s_r$ (%) |
| Na | 6802.1 | 45.6 | 542.6 | 8.2 |
| Mg | 6097.9 | 6.6 | 426.2 | 11.4 |
| Al | 4533.8 | 7.7 | 894.9 | 174.6 |
| Si | 3568.9 | 5.7 | 1170 | 138.6 |
| P | 2801.3 | 6.8 | 240.5 | 5.0 |
| K | 1217.6 | 5.6 | 131.5 | 3.3 |
| Ca | 1022.5 | 4.9 | 116.0 | 3.9 |
| Ti | 713.2 | 6.1 | 86.5 | 2.7 |
| Mn | 458.9 | 5.3 | 60.0 | 2.7 |
| Fe | 403.7 | 4.2 | 54.2 | 2.2 |
| Zn | 244.9 | 3.6 | 36.0 | 3.2 |
| Sr | 88.6 | 4.7 | 17.9 | 4.4 |

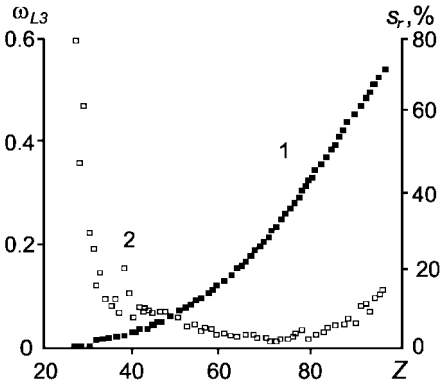


**Figure 3.** $\omega_{L3}$ (1) and $s_r$ (2) values versus atomic number.

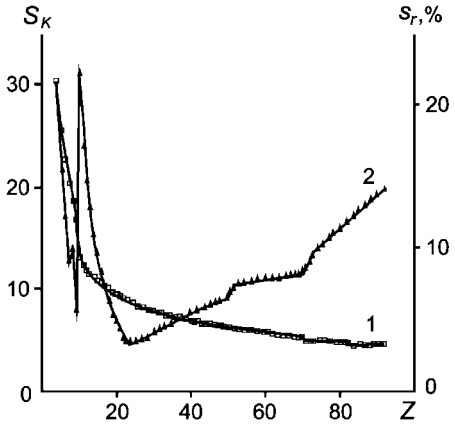


**Figure 4.** $S_K$ (1) and $s_r$ (2) values versus atomic number.

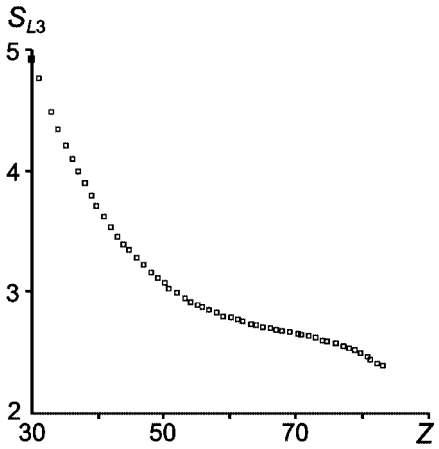


**Figure 5.** $S_{L3}$ value versus atomic number.

$L\alpha_2$, $L\beta_1$, $L\beta_3$ and $L\beta_4$ lines can be calculated for $Z = 29–92$, and of $L\beta_2$ and $L\gamma_1$ lines for $Z = 42–92$.

The relative intensities $R$ calculated using Eqn (18) are quite consistent with table data.

There is also a significant spread in absorption jump values represented in different sources. The average $S_K$ values are established on the basis of five papers, as well as the $s_r$ values. Figure 4 shows their dependence on $Z$. They are approximated by the Eqn (19):

$$S_K = 3.673 + 114.589Z^{-1} - 27.125Z^{-2} \tag{19}$$

The correlation coefficient for the formula and table data is 0.9946.

Figure 5 presents average $S_{L3}$ values versus $Z$. This relationship is approximated by the following formula:

$$S_{L3} = 2.255 - 17.061Z^{-1} + 2961.53Z^{-2} \tag{20}$$

The correlation coefficient for the formula and table data is 0.9989.

The absorption jumps of other sub-levels are taken as being equal to their average values in different sources: $S_{L1} = 1.18$, $S_{L2} = 1.4$, $S_{M1} = 1.07$, $S_{M2} = 1.11$, $S_{M3} = 1.32$, $S_{M4} = 1.32$.

## CALCULATIONS OF THE SPECTRAL INTENSITY OF X-RAY TUBE RADIATION

Based on Kramers' theory and Bethe's law for stopping power, the spectrum intensity of bremsstrahlung radiation $I_E$ can be expressed as follows:

$$I_E = \text{const} \times Z \int_{E_0}^{E} \frac{dE}{\ln(\alpha E)} \tag{21}$$

where $\alpha = 1.166/J$ and $J$ is the mean excitation energy.

Allowing for a weak dependence of $\ln(\alpha E)$ on $E$, we use a mean-value theorem and obtain a simple expression, with $E$ having some mean value, e.g. $\overline{E} = E_0/2$.[1] However, the $\ln(\alpha E)$ function increases sharply when the energy of electrons changes from 1 to 15 keV. When the XRF intensities are calculated for the Na K$\alpha$, Si K$\alpha$ and Fe K$\alpha$ lines, the function value changes, within the 1 to 50 keV energy interval, from 4.5 to 0.65, 1.26 and 2.61, respectively. So, taking $\overline{E}$, with the $\ln(\alpha E)$ function form ignored, entails serious calculation errors in the spectrum distribution of bremsstrahlung radiation determined by virtue of the mean-value theorem-derived formula.

Calculations are made to determine the $\overline{E}$ value providing for the least deviations of $F(E, \overline{E}) = (E_0 - E)/\ln(\alpha\overline{E})$ function with reference to $\varphi(E) = [\text{li}(\alpha E_0) - \text{li}(\alpha E)]/\alpha$ function derived from integration of Eqn (21). The mean energy value is determined as $\overline{E} = aE + bE_0$. With the $Z$ of the anode target, $E$, $E_0$ and $J$ values being changed, some $a$ and $b$ coefficient

**Table 5.** Calculation coefficients for line radiation probabilities

| Coefficients | $L\alpha_1$ | $L\alpha_2$ | $L\beta_2$ | $L\beta_1$ | $L\gamma_1$ | $L\beta_3$ | $L\beta_4$ |
|---|---|---|---|---|---|---|---|
| $a_0$ | 0.4961 | 0.0511 | −0.5955 | 0.3601 | −0.4308 | 0.1776 | 0.0940 |
| $a_1$ | −0.002 56 | −0.000 095 | 0.027 04 | −0.001 57 | 0.019 34 | −0.003 69 | −0.002 02 |
| $a_2$ | 0.000 009 | −0.000 001 | −0.000 37 | 0.000 003 | −0.000 259 | 0.000 049 | 0.000 03 |
| $a_3$ | 0 | 0 | $1.65 \times 10^{-6}$ | 0 | 0.000 001 | $-2.604 \times 10^{-7}$ | 0 |

values are calculated by virtue of the least-squares method. We use these data as a basis to derive an approximated formula for the mean electron energy, which provides for a minimum calculation error in the case of different targets, accelerating voltages and bremsstrahlung radiation energies:

$$\overline{E} = \frac{E_0 + 2E}{3} \tag{22}$$

Equation (22) is then used to calculate the spectrum distribution of the X-ray tube bremsstrahlung radiation:

$$N_\lambda = 3.85 \times 10^{-4} Z \frac{1}{\ln(\alpha \overline{E})} \left( \frac{1}{\lambda_0} - \frac{1}{\lambda} \right) \frac{1}{\lambda} Rf \exp\left(-\mu_0 \rho_0 d_0\right) \tag{23}$$

where $R$ is the backscatter correction factor, $f$ is the X-radiation absorption correction, $\mu_0$, $\rho_0$ and $d_0$ are the MAC, density and thickness of the Be window respectively.

The intensity of the characteristic radiation is calculated by the formula:

$$N_l = a_q \frac{1}{Z} \left\{ \frac{E_0}{E_q} - 1 - \frac{\ln(\alpha E_q)}{\alpha E_q} \left[ \mathrm{li}\,(\alpha E_0) - \mathrm{li}\,(\alpha E_q) \right] \right\} \times Rf \exp\left(-\mu_0 \rho_0 d_0\right) \tag{24}$$

The $a_q$ coefficient value depends on a $q$-series.

We use these formulas to calculate the spectra of two X-ray tubes: SEG-50 (Rh anode target, Be window thickness 0.120 mm, voltage 45 kV), and OEG-50 (W anode target, Be window thickness 1.0 mm, voltage 50 kV). A comparison of our calculation results with experimental data already published has demonstrated their satisfactory agreement. The calculation estimates of the contribution of the Rh anode target characteristic radiation, i.e. 25.44% for L lines and 9.6% for K lines, agree rather well with corresponding experimental values: 24.8% and 10.1%. The comparison of the results of the calculated and experimental data for the OEG-50 X-ray tubes with a W anode target were also satisfactory.

Equations (23) and (24) are used in calculations of the spectrum distributions of the OEG-75 H and 3PXB2 (Rh anode target) X-ray tube radiations, whose values are used to make measurements. The calculation results are presented in Fig. 6.

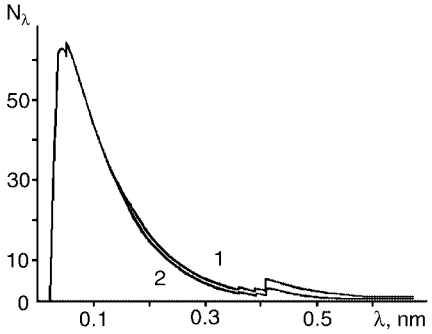


**Figure 6.** Calculation results of spectrum distribution of X-ray tube (Rh anode target) bremsstrahlung radiation $V_0 = 50$ kV: (1) OEG-75 H, $d_0 = 0.127$ mm; (2) 3PXB2, $d_0 = 0.250$ mm.

## IMPROVING THE CALCULATION ALGORITHM AND THE CALCULATION PROGRAM

When XRF analysis is based on the FP method, the bulk of the computer calculations is numerical integrations of wavelengths of the X-ray tube bremsstrahlung radiation, arising from Eqns (4) and (7). For a many-component sample, the functions for absorption in Eqn (4) and secondary XRF in Eqn (7) have first-type discontinuities in the range of integration. Hence, the integral for the entire integration range is represented as a sum of integrals with the number of its members equalling the number of sample elements, the absorption edge wavelengths of which are less than the absorption edge wavelength of the element determined. Correspondingly, the range of integration is divided into sub-ranges, where a numerical integration is performed in terms of a quadrature formula, usually Simpson's formula. Both the behaviour of the integrated function and the different contributions of the spectrum intervals to the sum of integrals provide for the required accuracy of the integration procedure, with a minimum

**Table 6.** Calculation errors of approximate integral values in sub-ranges, with Na determined in SGD-1A SRM sample

| Analytical line | Continuous spectrum interval | Errors versus number of quadrature nodes within an interval[a] (%) | | | | | | No. of nodes within an interval |
|---|---|---|---|---|---|---|---|---|
| | | 2 | 4 | 8 | 16 | 32 | 64 | |
| Na Kα | $\lambda_0 - \lambda_q^{Fe}$ | −0.005 | 0.004 | – | 0.006 | −0.001 | – | 32 |
| | $\lambda_q^{Fe} - \lambda_q^{Mn}$ | – | – | – | – | – | – | 8 |
| | $\lambda_q^{Mn} - \lambda_q^{Ti}$ | – | – | – | – | – | – | 2 |
| | $\lambda_q^{Ti} - \lambda_q^{Ca}$ | – | 0.004 | 0.002 | 0.001 | – | – | 2 |
| | $\lambda_q^{Ca} - \lambda_q^{K}$ | – | – | – | – | – | – | 4 |
| | $\lambda_q^{K} - \lambda_q^{P}$ | 6.14 | −4.26 | 0.34 | 0.82 | −0.15 | 0.34 | 8 |
| | $\lambda_q^{P} - \lambda_q^{Si}$ | −0.002 | – | 0.02 | 0.008 | – | 0.002 | 2 |
| | $\lambda_q^{Si} - \lambda_q^{Al}$ | −0.001 | – | – | – | – | – | 2 |
| | $\lambda_q^{Al} - \lambda_q^{Mg}$ | 0.004 | – | – | – | – | – | 2 |
| | $\lambda_q^{Mg} - \lambda_q^{Na}$ | 0.004 | – | – | – | – | – | 2 |

[a] Dash is an error less than 0.001%.

number of quadrature formula nodes within sub-ranges and throughout the entire integration range.

The errors of integration by the Simpson's quadrature formula are estimated for the XRF analysis of petrogenic elements in rocks and Fe–Ni–Cr alloys. In the case of petrogenic elements, the experimental conditions correspond to the determination conditions used in this study. Table 6 contains the relative calculation errors for approximate integral values to determine the Na content of SRM rock sample SGD-1A, established by the following formula:

$$\delta = \frac{I_n - I_{128}}{\sum_{i}^{k} (I_{128})_i} \times 100\% \qquad (25)$$

where $I_n$ and $I_{128}$ are the integral values for the absorption function with $n$ and 128 nodes for each integration sub-range respectively; $k$ is the number of sub-ranges $[\lambda_0, \lambda_q^i]$. According to Table 6, the node density is the highest within sub-ranges where an integrand function has the largest curvature and jumps; in this case, it is $[\lambda_q^{\mathrm{K}}, \lambda_q^{\mathrm{P}}]$. Such calculations have been made for all rock-forming elements. It should be noted that the errors within the same sub-ranges, but for different analytical lines, display an insignificant decrease, whereas the lines have a relative shift over the spectrum. This allowed us to use a constant number of nodes within a sub-range, irrespective of the element being determined. An optimum is the number of nodes within each sub-range and the entire range $[\lambda_0, \lambda_q^i]$ that provides for the calculation error not to exceed one-third of the determination error $\delta = s_{\mathrm{r,D}} t(n, P)$, where $s_{\mathrm{r,D}}$ is an allowable relative error.[20] The number of nodes in sub-ranges, which agrees well with this criterion, is given in the last column of Table 6.

The absorption function is calculated by two variants. In the first variant, an interval from $\lambda_0$ to the absorption edge of an element with the least $Z$ was divided into 400, 300, 200, 100 and 50 integration steps. In the second variant, this integration interval was divided into a number of sub-intervals equalling the number of elements determined. These sub-intervals were assigned with the combination of nodes given in Table 6. It was established that, in order to provide for an acceptable accuracy of calculation of all elements, there must be not less than 200 steps in the first variant. The second variant is preferable on account of its smaller time losses and it also provides for the least calculation errors for the Na, Mg, Al and Fe. Calculation errors for the Si, P and Ti elements are close to the calculation errors in the case of 300 quadrature nodes. On the whole, the calculation errors of the first variant are less than those allowable for all elements.

Wavelengths of sample microcomponent absorption edges are not regarded as the boundaries of integration areas, since low contents of such elements are insignificant for the character of the integrand functions.

For XRF analysis of Fe–Ni–Cr alloys, the optimization of the integration, by a continuous spectrum and under excitation conditions,[31] results in a node distribution through corresponding intervals as follows: $[\lambda_0, \lambda_{\mathrm{K}}^{\mathrm{Ni}}]$ of 16; $[\lambda_{\mathrm{K}}^{\mathrm{Ni}}, \lambda_{\mathrm{K}}^{\mathrm{Fe}}]$ of 2; $[\lambda_{\mathrm{K}}^{\mathrm{Fe}}, \lambda_{\mathrm{K}}^{\mathrm{Cr}}]$ of 2.

An MFPM program with a modified algorithm has been developed. It is aimed at calculating the intensities of the basic characteristic lines of the K-, L-, and M-series and the contents of elements having $Z$ from 11 to 92, in terms of measured intensities. The element weight fractions are calculated on-line and off-line. The best XRF analysis conditions were examined and selected; the intensities of the analytical lines of the elements were calculated for different conditions of radiation excitation and recording, sample preparation and for different matrices; all calculations were made in an interactive mode.

This program was used by us to calculate the XRF relative intensities of analytical lines of the main rock elements for homogenized samples obtained by fusion of powder samples with $Li_2B_4O_7$, in mass ratio 1 : 1. The analytical line intensities of Rb, Sr and Ba microelements are calculated for the initial powder samples. The reference sample is the MK-1 granodiorite SRM. The difference between measured and calculated values has $S_r$ equalling 0.85%, 2.1%, 3.0%, 6.0%, 9.1%, 7.4%, 13.7%, 16.0%, and 15.6% for the K$\alpha$ lines of Si, Al, Fe, Mg, Ca, K, Rb, and Sr, and L$\alpha$ lines of Ba, respectively.

The XRF intensities of K$\alpha$ lines of Fe, Ni and Cr were also calculated for their binary and tertiary systems. The set of nodes for this case is given above. The results obtained are compared with experimental data.[31] The difference between experimental and calculated relative intensities is designated as a random $x_i$ value. The results of the comparison between experimental and calculated intensities are presented in Fig. 7, as their difference histogram. The Fe and Ni data agree well, whereas the Cr data are systematic discrepant, due to the lower calculated intensities of the Cr K$\alpha_1$ line for nearly all Fe–Ni–Cr samples. In Fig. 7, such data are shown by a cross-hatched area. On the one hand, such a result testifies to the need for a program of the tertiary fluorescence effect correction to be introduced in the algorithm for such systems, and, on the other hand, it demonstrates the high accuracy of the calculations, which allows for identification of this effect.

On the whole, as the results of calculations made show, the optimization of the numerical integration procedure in terms of wavelengths of the X-ray bremsstrahlung radiation and the modification, on this basis, of the intensity calculation algorithm shows the adequacy of the XRF mathematical model.

The study results obtained have permitted us to use, for the first time, an algorithm of FP method, without simplification of the physical model, in order to make a

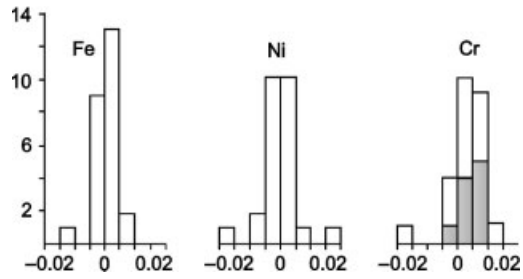


**Figure 7.** Divergence histograms of experimental and calculated relative intensities of Fe, Ni and Cr K$\alpha_1$ line radiation.

multiple XRF analysis on an SRM-25 spectrometer with a microcomputer.[32]

By now, the program has been adapted to be installed in a personal computer.

The time for evaluation of ten elements is of the order of several seconds and is much less than the time of measuring.

## AN XRF ANALYSIS OF ROCKS

### Preparation of rock samples

Two mutually complementary methods of sample preparation were used, which include homogenization of samples by their fusion with a flux. The first method is sample fusion with $Li_2B_4O_7$ flux, in mass ratio 1 : 1, grinding the alloy and forming a two-layered radiation source with boric acid base. Under the second method, homogeneous glass beads were obtained for use as the radiation source, and the sample to flux mass ratio was 1 : 2.[33]

### Experimental conditions

The ARL-72000 and SRM-25 spectrometers were used. The primary radiation sources were X-ray tubes with an Rh anode target. Accelerating voltage was 50 kV, current 40 mA, $\varphi = 90°$, $\psi = 30–40°$; sample measuring time 60–100 s. All elements were determined by their K$\alpha$ line, except for Ba, which was determined by the L$\alpha$ line.

### Metrologic characteristics

Table 7 contains $s_r$ and $s_{r,D}$, values and the accuracy potentials of $z$ values derived from the following formula: $z = s_{r,D}/s_r$.[20] Determinations of $Al_2O_3$, MgO, $Na_2O$ and $P_2O_5$ based on the FP method correspond to the accuracy criterion,[20] when the element contents of the samples are higher than 3.2%, 0.23%, 0.9% and 0.06% respectively, and for other oxides such a correspondence exists throughout the entire interval of contents given in Table 7.

**Table 7.** An assessment of reproducibility of petrogenic element determinations

| Oxide | Oxide content interval (%) | $s_r$ (%) | $s_{r,D}$ (%) | $z$ |
|---|---|---|---|---|
| $SiO_2$ | 40.0–99.0 | 1.0–0.5 | 1.0–0.7 | 1.0–1.4 |
| $TiO_2$ | 0.07–1.80 | 2.8–1.0 | 18.0–7.0 | 6.4–7.0 |
| $Al_2O_3$ | 0.2–3.2 | 28.0–8.0 | 25.0–8.0 | 0.9–1.0 |
| | 3.2–16.0 | 8.0–0.9 | 8.0–3.5 | 1.0–3.9 |
| $Fe_2O_{3tot}$ | 0.7–15.3 | 4.1–0.3 | 13.5–2.1 | 3.3–8.4 |
| MnO | 0.05–0.22 | 15.0–2.5 | 17.0–8.0 | 1.0–3.2 |
| MgO | 0.05–0.23 | 56.3–16.0 | 27.0–16.0 | 0.5–1.0 |
| | 0.23–32.4 | 16.0–1.6 | 16.0–1.8 | 1.0–1.1 |
| CaO | 0.1–11.0 | 19.0–1.0 | 21.0–3.2 | 1.1–3.2 |
| $Na_2O$ | 0.2–0.9 | 45.0–12.0 | 20.0–12.0 | 0.44–1.0 |
| | 0.9–5.4 | 12.0–4.8 | 12.0–5.4 | 1.0–1.2 |
| $K_2O$ | 0.04–4.7 | 21.7–0.7 | 23.0–8.0 | 1.0–11.4 |
| $P_2O_5$ | 0.01–0.06 | 43.8–12.0 | 21.9–12.0 | 0.49–1.0 |
| | 0.06–0.64 | 12.0–1.0 | 12.0–6.0 | 1.0–6.0 |

Oxides of Na, Mg, P, K, Ca, Ti, Mn and Fe have corresponding limits of detection as follows: 0.25, 0.06, 0.02, 0.02, 0.01, 0.007, 0.02, 0.04%.

The accuracy of determinations of petrogenic element contents is estimated by using SRMs of different rock types. Table 8 contains the $m$ number of SRMs, standard deviations, which represent the discrepancy between determined and confirmed content values, and the Student's $t$ coefficient. The error distribution obeys the normal law. No systematic errors were found.

Table 9 contains such parameters as reproducibility, accuracy of determinations, and limits of detection of Rb, Sr and Ba microelements obtained by using glass beads. All results are obtained only using the MK-1 granodiorite sample.

It follows from Table 9, that the XRF analysis based on the method discussed provides for a high reproducibility of determinations and has a great accuracy potential for corresponding content intervals.

The advantage of the FP method becomes quite obvious, when ultra-basic rocks are examined. If any other methods are used, it is difficult to select reference samples close in composition to an unknown sample to be examined, due to the low content of their alkalic elements, i.e. at the

**Table 8.** Statistical results on petrogenic elements determined in SRM rock samples

| Oxide | Oxide content interval (%) | $m$ | $s$ (%) | $t_{calc}$ |
|---|---|---|---|---|
| $SiO_2$ | 37.62–75.8 | 40 | 0.41 | 1.35 |
| $TiO_2$ | 0.017–6.99 | 39 | 0.035 | 0.13 |
| $Al_2O_3$ | 0.97–26.47 | 39 | 0.186 | 0.66 |
| $Fe_2O_{3tot}$ | 0.63–20.98 | 39 | 0.142 | 1.42 |
| MnO | 0.014–0.40 | 39 | 0.007 | 0.04 |
| MgO | 0.10–41.86 | 36 | 0.192 | 1.21 |
| CaO | 0.10–10.97 | 39 | 0.159 | 0.48 |
| $Na_2O$ | 0.72–13.33 | 37 | 0.136 | 1.02 |
| $K_2O$ | 0.10–7.18 | 37 | 0.090 | 1.77 |
| $P_2O_5$ | 0.03–2.21 | 32 | 0.014 | 1.54 |

**Table 9.** Metrologic characteristics of Rb, Sr and Ba determination methods using glass beads

| Characteristics | Rb | Sr | Ba |
|---|---|---|---|
| *Reproducibility* | | | |
| Content interval (ppm) | 20–120 | 70–1000 | 220–2400 |
| $s_r$ (%) | 12.1–3.0 | 2.9–1.0 | 9.0–1.0 |
| $s_{r,D}$ (%) | 30–25 | 30–19 | 30–19 |
| *Accuracy* | | | |
| Content interval (ppm) | 14–1100 | 20–2300 | 99–1900 |
| $m$ | 22 | 24 | 25 |
| $s_r$ (%) | 18.7 | 13.4 | 16.1 |
| $t_{calc}$ | 1.6 | 0.6 | 1.9 |
| *Limit of detection* | | | |
| $c_{min}$ (ppm) | 5.6 | 7.2 | 34 |

**Table 10.** The results of XRF analysis of ultra-basic rock samples (SRM), with different reference sample

| Sample | Note[a] | Oxide Content (%) | | | | | | | | | |
|---|---|---|---|---|---|---|---|---|---|---|---|
| | | $Na_2O$ | MgO | $Al_2O_3$ | $SiO_2$ | $P_2O_5$ | $K_2O$ | CaO | $TiO_2$ | MnO | $Fe_2O_{3tot}$ |
| MU-1 peridotite | 1 | 0.01 | 37.12 | 1.84 | 45.54 | 0.036 | 0.044 | 1.26 | 0.107 | 0.183 | 11.58 |
| | 2 | | 36.23 | 2.15 | 45.95 | 0.02 | | 1.55 | 0.07 | 0.183 | 10.98 |
| | 3 | | 36.80 | 2.10 | 45.21 | 0.02 | | 1.58 | 0.06 | 0.185 | 10.49 |
| MU-2 dunite | 1 | 0.048 | 42.40 | 0.32 | 35.07 | 0.027 | (0.025) | (0.22) | (0.056) | 0.176 | 10.06 |
| | 2 | | 42.23 | 0.38 | 36.42 | 0.02 | | 0.26 | | 0.173 | 10.06 |
| | 3 | | 42.49 | 0.39 | 35.57 | 0.01 | | 0.26 | | 0.171 | 9.53 |
| MU-3 hornblendite | 1 | 2.14 | 12.70 | 14.24 | 39.95 | 0.032 | 0.382 | 11.04 | 1.91 | 0.144 | 18.26 |
| | 2 | 2.18 | 12.79 | 14.43 | 38.60 | 0.02 | 0.36 | 10.99 | 1.98 | 0.151 | 18.45 |
| | 3 | 1.95 | 12.95 | 14.02 | 38.30 | 0.02 | 0.36 | 11.31 | 1.93 | 0.150 | 17.74 |
| MU-4 kimberlite | 1 | 0.087 | 26.96 | 2.66 | 37.66 | 0.216 | 0.412 | 6.42 | 0.97 | 0.111 | 7.57 |
| | 2 | | 25.82 | 2.61 | 37.03 | 0.22 | 0.38 | 6.52 | 0.97 | 0.094 | 7.44 |
| | 3 | | 26.11 | 2.59 | 36.88 | 0.17 | 0.38 | 6.69 | 0.95 | 0.096 | 7.18 |

[a] 1: a certified content; 2, 3: determination results of reference samples MK-1 (granodiorite) and SGD-1A (gabbro).

threshold limit of detection level. The FP method does not encounter such a problem, and such rocks are examined by one reference sample only.

Table 10 contains petrogenic element contents determined using different reference samples and compares then with confirmed data for SRMs of ultra-basic rocks. The analytical results are independent of the reference samples selected and demonstrate the validity of matrix effects under the contents calculation program.

## CONCLUSION

In order to improve the model of characteristic X-ray radiation, when rock samples are analysed, the role of photoelectrons is examined in detail, and the effects of the primary radiation beam divergence are assessed. The FP uncertainties are studied, and equations are proposed to calculate the fluorescence yield, probabilities of series line radiation and absorption jumps; equations are also proposed to calculate the mean electron energy and the X-ray tube spectrum distribution. An algorithm for numerical integration by wavelengths is optimized, with contribution of X-ray tube bremsstrahlung radiation accounted for. A program is developed to calculate the characteristic radiation intensities and element contents. The metrologic characteristics of the FP-based XRF method allow for its use in making routine examinations of rocks.

### Acknowledgements

The author thanks T.I. Velicoda for her translation of this article from Russian into English. Especially acknowledged is the help of V.I. Manuilova and O.N. Tunin.

## REFERENCES

1. Afonin VP, Finkelshtein AL, Borkhodoev VYa, Gunicheva TN. *X-Ray Spectrom.* 1992; **21**: 69.
2. Sherman J. *Spectrochim. Acta* 1955; **7**: 283.
3. Pavlinsky GV, Losev NF. *Zavod. Lab.* 1963; **29**: 1067.
4. Shiraiwa T, Fujino N. *Jpn. J. Appl. Phys.* 1966; **5**: 886.
5. Afonin VP, Gunicheva TN. *X-Ray Fluorescence Analysis of Rocks and Minerals*. Nauka: Novosibirsk, 1977 (in Russian).
6. Pavlinsky GV, Gulayev VT. *Investigations in the Field of Physics of Solids*, Vol. 2. Irkutsk State University: Irkutsk, 1974; 230.
7. Afonin VP, Gunicheva TN, Piskunova LF. *X-ray Fluorescence Silicate Analysis*. Nauka: Novosibirsk, 1984 (in Russian).
8. Pavlinsky GV, Yu Dukhanin A. *X-Ray Spectrom.* 1994; **23**: 221.
9. Pavlinsky GV, Kitov BI. *X-Ray Spectrom.* 1979; **8**: 96.
10. Leroux J. *Adv. X-Ray Anal.* 1962; **5**: 153.
11. Heinrich KFJ. *The Electron Microprobe*. Wiley: NewYork, 1966.
12. Theisen R, Togel K, Vollath D. *Mikrochim. Acta* 1967; **2**: 16.
13. Dewey RD, Mapes RS, Reynolds TW. *Handbook of X-Ray and Microanalysis Data*. Pergamon Press: New York, 1969; 321.
14. Storm E, Israel H. *Nucl. Data Tables* **A7**: 1970; 565.
15. Thinh TP, Leroux J. *X-Ray Spectrom.* 1979; **9**: 85.
16. Henoc J, Tong M. MBXCOR a new package for the automatic CAMEBAX microprobe. *Cameca News*, 1980.
17. Marenkov OS. *X-Ray Spectrometry Tables and Formulas*, Vol. 3. Mashinostroenie: Leningrad, 1982 (in Russian).
18. Heinrich KFJ. *11th International Congress on X-Ray Optics and Microanalysis*, 1986; 67.
19. de Boer DKG. *Spectrochim. Acta Part B* 1989; **44**: 1171.
20. Ostroumov GV (ed.). *Methods of Studying Chemical Compositions of Rocks, Ores and Minerals*. Nedra: Moscow, 1979 (in Russian).
21. Wentzel G. *Z. Phys.* 1927; **43**: 524.
22. Bambynek W, Grasemann B, Fink RW, *et al*. *Rev. Mod. Phys.* 1972; **44**: 716.
23. Burhop EHS, Assad WN. *Adv. Atom. Mol. Phys.* 1972; **8**: 163.
24. Freund H. *X-Ray Spectrom.* 1975; **4**: 90.
25. Krause MO. *J. Phys. A: Chem. Ref. Data.* 1979; **8**: 307.
26. Blokhin MA, Shveizer IG. *Handbook of X-Ray Spectrometry Data*. Nauka: Moscow, 1982 (in Russian).
27. Bambynek W. *Proceedings of X-ray and Inner-Shell Processes in Atoms, Molecules and Solids*, Leipzig, 20–24 August, 1984.
28. Hanke W, Wernisch J, Pöhn C. *X-Ray Spectrom.* 1985; **14**: 43.
29. Pöhn C, Wernisch J, Hanke W. *X-Ray Spectrom.* 1985; **14**: 120.
30. Broll N. *X-Ray Spectrom.* 1986; **15**: 271.
31. Rasberry SD, Heinrich KFJ. *Anal. Chem.* 1974; **46**: 81.
32. Borkhodoev VYa. *Zh. Anal. Khim.* 1992; **47**: 438.
33. Borkhodoev VYa. *Patent Russian Federation* No. 2098791, 1995.